Adsorption Dynamics and Electrochemical and Photophysical Properties of Thiolated Ruthenium 2,2′-Bipyridine Monolayers

Paolo Bertoncello,[†] Evangelos T. Kefalas,[‡] Zoe Pikramenou,*[,‡] Patrick R. Unwin,*[,†] and Robert J. Forster*[,§]

Department of Chemistry, University of Warwick, Coventry CV4 7AL, United Kingdom, School of Chemistry, University of Birmingham, Edgbaston B15 2TT, United Kingdom, and National Center for Sensor Research, School of Chemical Sciences, Dublin City University, Dublin 9, Ireland

Received: December 13, 2005; In Final Form: March 8, 2006

A new complex $[Ru(bpy)_2(bpySH)](PF_6)_2$, RuBpySH, has been prepared bearing two anchoring groups for surface attachment, where bpy is 2,2′-bipyridyl and bpySH is 5,5′-bis(mercaptomethyl)-2,2′-bipyridine. Monolayers of RuBpySH have been formed on micro and macro platinum electrodes by spontaneous adsorption from micromolar solutions of the complex in 50:50 v/v water/acetone. The monolayers can be reversibly switched between the Ru^{2+} and the Ru^{3+} forms. Cyclic voltammetry is well-defined with a peak-to-peak splitting of 30 ± 5 mV and a full width at half-maximum of 110 ± 10 mV being observed for scan rates up to 5 V s^{-1} where the supporting electrolyte is 0.1 M tetrabutylammonium tetrafluoroborate in acetonitrile. Adsorption is irreversible in this system, and the saturation coverage obtained is $8.1 \pm 0.4 \times 10^{-11}$ mol cm^{-2} when the complex concentration in the deposition solution is between 10 μM and 1.0 mM. The dynamics of adsorption depend markedly on the bulk concentration and are described in terms of irreversible adsorption. Dry monolayers display luminescence properties similar to those of powder samples of the complex, indicating that the monolayer has characteristics of the solid-state sample rather than the solution sample of the complex. Significantly, efficient electrochemiluminescence is generated using tripropylamine as the coreactant. The rate of electron transfer across the electrode/monolayer interface has been probed using high scan rate cyclic voltammetry. The standard heterogeneous electron-transfer rate constant, $k°$, is $0.9 \pm 0.1 \times 10^4$ s^{-1}, and there is weak adsorbate−electrode electronic communication.

Introduction

Self-assembly of a monolayer involves the spontaneous coordinated action of independent building blocks to create a superstructure.[1,2] This process is of great importance in biology, chemistry, and supramolecular nanotechnology. In particular, for the purpose of nanofabrication, self-assembly is envisaged as an important avenue for the "bottom-up" fabrication of supramolecular nanostructures with useful properties. While the structure and properties of equilibrated assemblies are now well-understood, there are outstanding issues regarding the kinetics of the monolayer formation process.[3] The principal techniques that have been used to probe adsorption dynamics include quartz crystal microbalance studies,[4,5] contact angle measurements,[6] ellipsometry, reflectance absorption infrared spectroscopy,[7] surface plasmon resonance,[8] surface second harmonic generation,[9] and atomic force microscopy.[10] However, when the molecular building block is redox-active, electrochemical techniques can provide a powerful insight not only into the surface coverage of individual species but also their adsorption strength and chemical reactivity.[11−13]

In this paper, we report the synthesis of a new surface-active Ru(II) complex, $[Ru(bpy)_2(bpySH)]^{2+}$, denoted RuBpySH, Scheme 1, where bpy is 2,2′-bipyridyl and bpySH is 5,5′-bis-

SCHEME 1

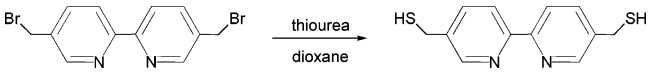

(mercaptomethyl)-2,2′-bipyridine. We also report on the spontaneous adsorption dynamics and redox and (electrochemi)-luminescent properties of monolayers. The electrochemical responses of these monolayers are unusually ideal, allowing the time dependence of the surface coverage to be conveniently monitored as the monolayer assembles.

One of the motivations behind the formation of films of this kind is to probe their capacity to efficiently generate electrochemiluminescence. For example, we recently reported that the oxidation of guanines in DNA by electrochemically generated $[Ru(bpy)_2(PVP)_{10}]^{2+}$ in ultrathin *polymer* films leads to photoexcited $[Ru(bpy)_2{}^{2+}]$* sites in the film that generate electrochemiluminescence (ECL) upon relaxation back to the ground state, where PVP is poly(4-vinylpyridine).[14] This thin-film ECL approach has been exploited to detect DNA damage induced by styrene oxide. We have also demonstrated that ultrathin films containing $[Os(bpy)_2(PVP)_{10}]^{2+}$ and oligonucleotides on electrodes can directly generate ECL to detect oxidized guanines in DNA without using a sacrificial reductant.[15] However, when seeking to create efficient ECL platforms using monolayers, quenching of the emission by the metallic states of the electrode represents a significant challenge. Here, we report that efficient ECL can be observed from systems of this kind provided that the monolayers are given sufficient time to anneal and the extent of electronic coupling between electrode and adsorbate is low.

* Authors to whom correspondence should be addressed. E-mail: z.pikramenou@bham.ac.uk; P.R.Unwin@warwick.ac.uk; robert.forster@dcu.ie.
[†] University of Warwick
[‡] University of Birmingham
[§] Dublin City University.

10.1021/jp057276j CCC: $33.50
Published on Web 05/03/2006

We have chosen a functionalized Ru(II) tris-bipyridyl complex with two thiol anchoring groups for surface attachment due to its attractive luminescent and electrochemical properties. This complex allows a directed assembly onto the surface in a rigid conformation that has particular advantages over previously reported mono- or polyfunctionalized Ru(II) thiol complexes.[16−18]

Experimental Section

Apparatus. Cyclic voltammetry was performed using a CH Instruments model 660 electrochemical workstation and a conventional three-electrode cell. Potentials are all referenced against a BAS nonaqueous silver/silver Ion (Ag/Ag^+) reference containing 0.005 M silver nitrate or perchlorate and 0.1 M tetrabutylammonium tetrafluoroborate ($TBABF_4$) electrolyte dissolved in acetonitrile. Microelectrodes were prepared using platinum microwires (Goodfellow) sealed in a glass shroud that were mechanically polished as described previously.[19] Electrochemical cleaning of the electrodes was carried out by cycling in 0.1 M H_2SO_4 between potential limits chosen to initially oxidize and then reduce the surface of the platinum electrode. Excessive cycling was avoided to minimize the extent of surface roughening. The geometric area of the electrodes was determined by recording cyclic voltammograms for $[Ru(NH_3)_6]^{2+}$ dissolved in solution under radial and semi-infinite linear diffusion conditions. To determine the surface roughness, the real, or microscopic, area of the electrodes was determined by calculating the charge under the peaks associated with platinum oxide reduction and hydrogen adsorption/desorption. Analysis of both processes yielded indistinguishable results, and typical surface roughness values were between 1.6 and 2.0.

An Oriel model IS520 gated intensified charge coupled device (CCD) operated at −20 °C, coupled to an Oriel model MS125 spectrograph, was used to acquire ECL spectra. All solutions were thoroughly degassed using nitrogen or argon prior to measurements. During experiments the cell was placed inside a specially constructed holder that positioned the working electrode in a reproducible manner directly opposite the face of a fiber optic bundle, the other end of which was coupled to the CCD. The entire electrode assembly was contained inside a light-tight box.

The luminescence studies were performed on a Quanta-Master QM-1 steady-state emission spectrometer from PhotonTechnology Instruments equipped with a 75 W xenon arc lamp and a model 810 photon-counting detection system with a red-sensitive R928 photomultiplier tube.[20,21] The luminescence spectra were not corrected for photomultiplier response due to the weak signal. The excitation spectrum was corrected for lamp and instrument response.

NMR spectra were recorded on either Brüker AC 300, AV 300, AMX 400, or AV 400 spectrometers. Chemical shifts are given in parts per million (ppm), and coupling constants (J) are given in Hertz (Hz). Electron impact mass spectra were recorded on a VG Prospec mass spectrometer. Elemental analyses were recorded on a Carlo Erber EA1110 Simultaneous CHNS elemental analyzer.

Materials and Procedures. All materials were purchased from Acros/Fisher with the exception of 5,5′-dimethyl-2,2′-bipyridine and 2,2′-bipyridine, which were purchased from Aldrich. $RuCl_3 \cdot xH_2O$ was supplied by Johnson-Matthey.

Synthesis of 5,5′-Bis(mercaptomethyl)-2,2′-bipyridine (bpySH). A solution of 5,5′-bisbromomethyl-2,2′-bipyridine[22] (200 mg, 0.58 mmol) and thiourea (123 mg, 1.61 mmol) in dry dioxane (30 mL) was brought to reflux under N_2 for 3 h. The reaction mixture steadily changed from pale to cloudy white, within the first 10 min. After 3 h NaOH (80 mg, 2 mmol) dissolved in 10 mL of degassed water was added, and the mixture was heated to reflux for another 3 h, during which there was a color change to clear yellow. The solvent was reduced in vacuo to yield a yellow material as the crude product. Approximately 25 mL of degassed acidified H_2O (pH ∼4, HCl) was added, and the aqueous phase was extracted with CH_2Cl_2 (5 × 40 mL). The organic phase was collected, and the solvent was removed in vacuo, yielding 0.12 g (82.8% yield) of a yellow solid, which was kept under N_2. ^{1}H NMR (300 MHz, $CDCl_3$, δ): 1.84 (t, 2 H, $J = 7.7$, −S**H**), 3.81 (d, 4 H, $J = 7.7$, −C**H**$_2$), 7.85 (dd, 2 H, $^3J = 8.0$, $^4J = 2.2$, H-4,4′), 8.40 (d, 2 H, $^3J = 8.0$, H-3,3′), 8.63 (s, 2 H, H-6,6′). ^{13}C NMR (75 MHz, CD_3CN, δ): 26.0 (−**C**H$_2$), 121.2 (C-3,3′), 137.5 (C-4,4′), 138.7 (C-5,5′), 149.7 (C-6,6′), 152.3 (C-2,2′). ES-MS (MeOH): m/z 249 $[M + H]^+$. Anal. Calcd for $C_{12}H_{12}N_2S_2$: C, 58.2; H, 4.9; N, 11.3. Found: C, 58.0; H, 4.9; N, 11.3.

Synthesis of $[Ru(bpy)_2(bpySH)](PF_6)_2$. $Ru(bpy)_2Cl_2 \cdot 2H_2O$[23] (130.9 mg, 0.25 mmol) and bpySH (93.0 mg, 0.37 mmol) were heated to reflux overnight, under nitrogen in degassed ethanol (15 mL). The solution was set aside to cool to room temperature, and a saturated methanolic solution of ammonium hexafluorophosphate (203.4 mg, 1.25 mmol) was added. The flask was placed in an ice−water bath for 120 min to promote precipitation. The brown-orange precipitate formed was collected by filtration, washed with degassed ethanol (2 × 5 mL), degassed water (2 × 5 mL), and ether (5 mL), and stored under nitrogen. Yield: 194 mg (82%).^{1}H NMR (300 MHz, CD_3CN, δ): 8.50 (d, $J = 8.2$, 4H, H_{bpy}-3,3′), 8.40 (d, $J = 8.4$, 2H, H_{bpySH}-3,3′), 8.05 (m, 4H, H_{bpy}-4,4′), 8.01 (dd, $J = 8.8$, H_{bpySH}-4,4′), 7.71 (m, 4H, H_{bpy}-6,6′), 7.61 (s, 2H, H_{bpySH}-6,6′), 7.39 (m, 4H, H_{bpy}-5,5′), 3.59 (d, $J = 8.4$, 4H, −C**H**$_2$). ^{13}C NMR (100 MHz, CD_3CN, δ): 25.6 ((−CH_2), 124.8 (C_{bpySH}-3,3′), 125.2 (C_{bpy}-3,3′), 128.4 (C_{bpy}-5,5′), 138.4 (C_{bpySH}-4,4′), 138.7 (C_{bpy}-4,4′), 143.0 (C_{bpySH}-5,5′), 151.6 (C_{bpySH}-6,6′), 152.6 (C_{bpy}-6,6′), 156.2 (C_{bpySH}-2,2′), 158.0 (C_{bpy}-2,2′). ES MS (MeOH): m/z 807 $\{M - [PF_6]\}^+$, 331 $\{M - 2[PF_6]\}^{2+}$. UV−Vis λ in nm (log ϵ): 247 (4.60), 292 (4.89), 450, 420 (sh) (4.14). Anal Calcd for $RuC_{32}H_{28}N_6S_2P_2F_{12}$: C, 40.3; H, 2.9; N, 8.8. Found: C, 40.3; H, 2.9; N, 9.0.

Formation of Monolayers. Spontaneously adsorbed monolayers were formed upon immersion of the platinum (micro)-electrode in solutions of the complex in 50:50 H_2O/acetone at the concentrations between 10 μM and 1.0 mM. All deposition solutions containing RuBpySH were deoxygenated using nitrogen. Before electrochemical measurements were made, the electrodes were rinsed with Milli-Q water and the electrolyte to remove any unbound material. Subsequent measurements were performed in blank electrolyte.

Results and Discussion

Synthesis and Characterization. The bpySH ligand was prepared based on the transformation of a bromomethyl group to mercaptomethyl using thiourea[24] in a modified procedure that successfully led to bis-functionalization of the bipyridine (Scheme 1). The RuBpySH complex (Chart 1) was prepared in good yield using established ruthenium chemistry. A space-filling model is presented (Chart 1) based on a Ru(II) tris-bipyridyl structure. The electrospray mass spectrum shows characteristic peaks at m/z 331 and 807 corresponding to $\{M - 2[PF_6]\}^{2+}$ and $\{M - [PF_6]\}^+$, respectively. The complex has been fully characterized by ^{1}H and ^{13}C NMR spectroscopy. Its absorption spectrum displays the characteristic broad ^{1}MLCT band at 450 nm with a shoulder at 420 nm. Acetonitrile solutions

CHART 1

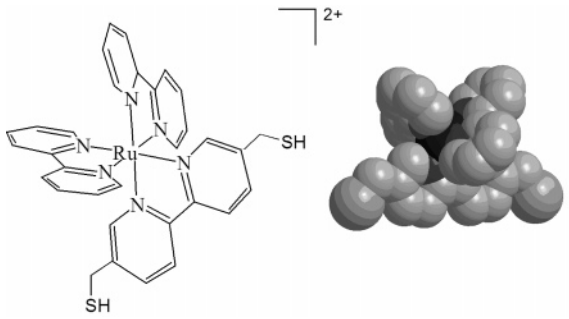

of the complex display strong luminescence from the ^{3}MLCT band when excited at 450 nm with a lifetime of 280 ns (aerated) and 770 ns (degassed) and a quantum yield of 1.1%. The excitation spectrum closely matches the absorption spectrum of the complex.

General Electrochemical Properties. Figure 1 illustrates the scan rate dependence of the voltammetric response of a 50 μm radius platinum microelectrode following 30 h of immersion in a 50 μM solution of RuBpySH dissolved in 50:50 H_2O/acetone. The scan rates, υ, are, from top to bottom, 5, 10, 50, and 100 V s^{-1}. The supporting electrolyte is 0.1 M $TBAPF_6$ in acetonitrile. For υ < 200 V s^{-1}, the response observed is consistent with that expected for an electrochemically reversible reaction involving a surface-confined reactant. For example, when species are adsorbed on an electrode surface, a peak-to-peak splitting, ΔE_p, of 0 mV and a full width at half-maximum (fwhm) of 90.6/n mV, where n is the number of electrons transferred, are expected where there are no interactions between adsorbates. The RuBpySH system exhibits an experimental ΔE_p of 15 ± 5 mV and a fwhm of 110 ± 10 mV, indicating that while there are destabilizing lateral interactions between adsorbates, close to ideal reversible behavior is observed.

Figure 1 shows that the peak shape is independent of the scan rate. Moreover, the inset of Figure 1 shows that the peak current, i_p, increases proportionally to the scan rate, which is consistent with an adsorbed rather than a diffusing reactant where i_p would be proportional to $\upsilon^{1/2}$. Also, the peak-to-peak separation remains constant with increasing scan rate, indicating that an ohmic drop and the dynamics of heterogeneous electron transfer do not influence the observed response at these time scales.

Dynamics of Monolayer Formation. An advantage of redox-active monolayers is that the adsorption process can be

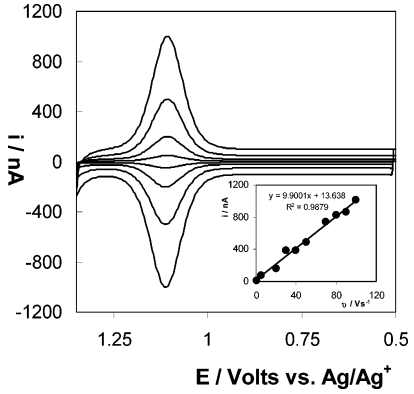

Figure 1. Cyclic voltammograms for a spontaneously adsorbed monolayer of RuBpySH in 0.1 M $TBAPF_6$ in acetonitrile. Scan rates are (top to bottom) 100, 50, 10, and 5 V s^{-1}. The radius of the platinum microelectrode is 50 μm. The monolayer surface coverage is 8.1 × 10^{-11} mol cm^{-2}. Cathodic currents are up, and anodic currents are down.

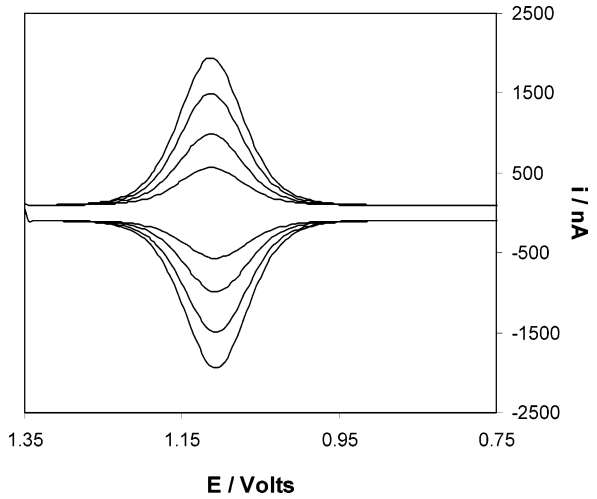

Figure 2. Dependence of the cyclic voltammetry response of a 50 μm in diameter Pt microelectrode following monolayer deposition for 90, 220, 420, and 1100 min from a 100 μM solution of RuBpySH. The voltammograms are recorded in blank acetonitrile containing 0.1 M $TBAPF_6$ as the supporting electrolyte. Cathodic currents are up, and anodic currents are down.

conveniently monitored using cyclic voltammetry.[1,2] Figure 2 illustrates the time evolution of the cyclic voltammogram obtained for a 50 μm diameter Pt microlectrode following monolayer deposition for 90, 220, 420, and 1100 min from a 100 μM solution of RuBpySH. Each voltammogram was recorded after washing and transfer to blank 0.1 M $TBAPF_6$ in acetonitrile. Figure 2 shows that the peak current increased slowly over a period of approximately 18 h. For this bulk concentration of complex in the deposition solution, the time required for mass transport of sufficient material to form a monolayer under linear diffusion conditions is approximately 100 ms, indicating that mass transport to the surface is not rate determining.

The surface coverage, Γ, can be determined from the area under the voltammetric peak after correcting for double-layer charging according to eq 1

$$\Gamma = \frac{Q}{nFA} \tag{1}$$

where Q is the total charge required to reduce or oxidize the electroactive species, n is the number of electrons transferred, F is Faraday's constant, and A is the area of the electrode.

Figure 3 illustrates the time dependence of the surface coverage where the bulk concentrations of the complex are 10 μM, 100 μM, and 1 mM. Significantly, this figure reveals that the saturation coverage, Γ_{sat}, observed at long deposition times is independent of the bulk concentration with a Γ_{sat} of 8.1 ± 0.4 × 10^{-11} mol cm^{-2} being observed. This limiting surface coverage corresponds to a molecular area of occupation of 205 ± 9 Å^2. This area is somewhat larger than that expected on the basis of the projected area of the bipyridine complex, 90 Å^2, suggesting that a close-packed monolayer is not formed even for high bulk concentrations and long deposition times. Consistent with the broadened voltammetric peaks observed, this behavior is most likely associated with repulsive electrostatic interactions between adjacent adsorbates and the need to incorporate charge-compensating counterions and solvent within the monolayer film. Alternatively, it is possible that the adsorbate adopts a skewed orientation because only one of the available thiols interacts with the surface. Future reports will

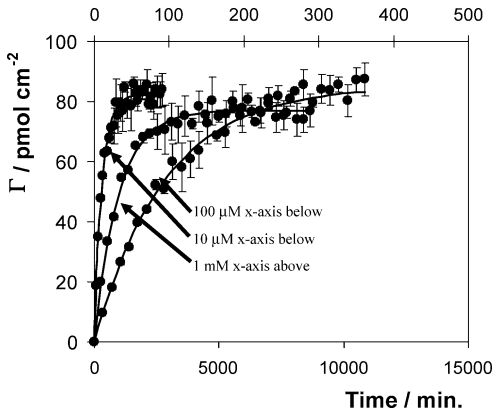

Figure 3. Time dependence of the surface coverage on the bulk concentration of RuBpySH. The individual surface coverages were measured electrochemically in blank electrolyte consisting of 0.1 M $TBAPF_6$ in acetonitrile. The solid lines represent the best fit to the Langmuir irreversible adsorption model.

address this issue using resonant Raman and surface-enhanced resonant Raman microscopy.

Figure 3 also reveals that the dynamics of adsorption depend markedly on the bulk concentration of the complex; e.g., the time taken to achieve the saturation coverage increases from approximately 250 min to more than a week when the bulk concentration is decreased from 1 mM to 10 μM. Given that mass transport is not rate limiting, this observation indicates that the binding kinetics depend on the bulk concentration. Analysis of the surface coverage versus time profiles can be used to measure rate constants and obtain more detailed insight into the monolayer formation mechanism. We have fitted a wide range of models to the surface coverage versus time data obtained at bulk concentrations of RuBpySH ranging from 10 μM to 1 mM. In each case, the sum square of the residuals between the experimental surface coverages and those predicted by the model were minimized using a gradient search algorithm. It is important to note that RuBpySH binds irreversibly to the platinum electrode surface. For example, irrespective of the bulk concentration used to form the monolayer, once the saturation coverage is attained the surface coverage decreases by less than 5% over a 2 day period when left in contact with 0.1 M $TBAPF_6$ dissolved in acetonitrile.

A consequence of adsorption being kinetically controlled is that the concentration of the adsorbing species adjacent to the surface approaches that found in bulk solution. Under these conditions, the rate of adsorption is first-order in the adsorbing species and first-order in the free sites at the surface (Langmuir-like behavior)

$$\frac{\partial \Gamma}{\partial t} = k_{ads} C_b (\Gamma_{sat} - \Gamma) \qquad (2)$$

where k_{ads} is the rate constant for adsorption and C_b is the bulk concentration of the surface-active complex.

Equation 2 can be integrated to give the coverage with time, assuming C_b and k_{ads} are independent of time or surface coverage.

$$\Gamma(t) = \Gamma_{sat}(1 - \exp(-k_{ads} C_b t)) \qquad (3)$$

Figure 3 shows that eq 3 is capable of reproducing the experimental time evolution in the surface coverage of RuBpySH. Significantly, the best-fit rate constant, 0.54 ± 0.04 $M^{-1}\ s^{-1}$, is independent of the bulk concentration for 10 μM < C_b < 1 mM. The fact that the rate constant is independent of C_b further confirms the appropriateness of this model.

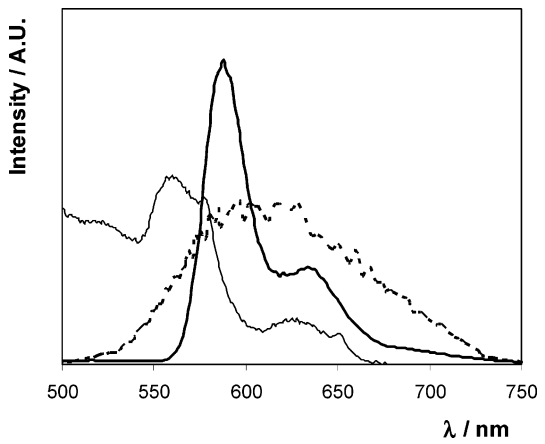

Figure 4. Emission spectra of a dry RuBpySH monolayer on a 3 mm Pt electrode (thin solid line), $\lambda_{exc} = 290$ nm. Emission spectra of RuBpySH at 77 K in butyronitrile/acetonitrile 4:1 solution (thick solid line). ECL spectra (- - -) from an RuBpySH monolayer ($\Gamma = 5 \times 10^{-11}$ mol cm^{-2}) recorded following a potential step to 1.20 V. The solution contains 0.1 M $TBABF_4$ in acetonitrile and 0.1 M tripropylamine.

It is important to emphasize that a wide range of alternative models were fitted to the data. These models included: (i) a second-order model where the rate-determining step involves a second reactant, e.g., displacement of a preadsorbed ion or solvent molecule, (ii) competing first-order dynamics characterizing adsorption where two pathways, e.g., two different orientations, exist, (iii) equilibrium models in which the initial adsorption process involves a weakly bound species that is in equilibrium with the bulk concentration followed by irreversible binding described by first-order kinetics. However, these alternative models either failed to replicate the experimentally observed behavior, giving plots of Γ_{model} versus Γ_{expt} that were systematically biased with respect to deposition time, i.e., exhibit slopes that are substantially different from unity or showed large positive or negative intercepts, or involved additional terms not needed to model the data.

It is also perhaps important to note that the accepted mechanism for the adsorption of alkane thiols onto gold proceeds by a two-step mechanism in which initial rapid physisorption is followed by monolayer annealing and the formation of a dense close-packed structure.[6,25] The data presented in Figure 3 involve surface coverages that are electrochemically determined. Data of this kind accurately measure the total number of moles of RuBpySH immobilized but do not provide an unambiguous insight into the orientation of the adsorbates or the monolayer structure. Thus, it is entirely possible that adsorption of RuBpySH follows the same two-step adsorption mechanism of alkane thiols; i.e., there may well be an intermediate disorganized liquid phase that precedes the formation of an organized solid film. The time constant for formation of an RuBpySH monolayer is comparable to that found for simple alkane thiols. The rate of alkane thiol adsorption depends on the chain length, but the initial rapid adsorption process leading to the formation of the "striped" phase takes on the order of 600−800 s, while annealing can take a further 50−60 h where the bulk concentration is 1 mM.

Photophysical Properties. To further investigate the properties of the RuBpySH monolayers, we have conducted luminescence experiments. Figure 4 shows that excitation of a dry RuBpySH monolayer leads to a broad emission with maxima at 560 and 630 nm. Figure 4 also shows the emission spectrum

of the complex in a butyronitrile/acetonitrile 4:1 glass at 77 K. While the emission maximum of the main component is shifted to lower energy by approximately 30 nm, the overall emission envelope for the complex in a solid glass and dry monolayers are broadly similar. Powder samples of RuBpySH display similar emission profiles. In the case of both the dry monolayers and the solids, excitation at 290 nm produces the most intense emission. The emission profile is characteristic of Ru(II) tribipyridyl complexes, attributed to the closely lying levels of the excited state.[26,27]

The observation that monolayers deposited on platinum are not completely quenched by electron transfer from the excited state into the electrode is significant and opens up the possibility of detecting biomolecules using electrochemiluminescence.[14,15] Electrochemiluminescence involves the creation of an electronically excited state through a redox reaction. For example, in solution electrogenerated $[Ru(bpy)_3]^{3+}$ emits at approximately 600 nm upon reaction with oxalate or tripropyl amine.

ECL from the monolayer-modified electrode was generated via the coreactant pathway using tripropylamine dissolved in acetonitrile containing 0.1 M $TBABF_4$. In the tripropylamine acid (TPA) reaction sequence, oxidation is believed to result in the formation of a short-lived radical cation, which then loses a proton to form a strongly reducing intermediate[28]

$$TPA - e^- \rightarrow TPA^+ \rightarrow (C_3H_7)_2N(C^{\bullet}HC_2H_5) + H^+ \quad (4)$$

This radical is then available to react with the oxidized form of the luminophore to produce the Ru^{2+*} excited state. When the potential of the electrode, in contact with such a solution, is held at 1.2 V, a faint but constant orange luminescence is observed originating from the layer. Figure 4 illustrates ECL spectra for a monolayer in which the surface coverage is 5×10^{-11} mol cm^{-2} after 48 h soaking in acetonitrile containing 0.1 M $TBAPF_6$. The spectrum was recorded in the absence of any dissolved complex. While there is significant noise in the data due to the small quantity of emissive material, a measurable emission centered at approximately 605 nm is observed. Significantly, the emission profile differs significantly from that observed for the dry monolayers and solid and is very similar to that observed for the complex dissolved in solution. This observation suggests that the monolayers become highly solvated when in contact with acetonitrile. The wavelength of maximum emission is similar to that observed for the complex dissolved in solution and is consistent with that found for the parent, $[Ru(bpy)_3]^{2+}$. Both the light-induced and the electrochemiluminescence data indicate that monolayers of $[Ru(bpy)_2(bpySH)](PF_6)_2$ emit, suggesting that the excited state is not strongly electronically coupled to the electrode surface. We probe the issue of electronic communication further in the following section by measuring the rate constant for heterogeneous electron transfer.

Heterogeneous Electron-Transfer Dynamics. The thiolated 2,2′-bipyridyl bridging ligand is not electrochemically innocent; e.g., bipyridyls are well-known to undergo two one-electron reduction reactions at potentials more negative than −1.8 V. Redox-active bridging ligands offer the possibility of significant virtual coupling (superexchange) depending on the difference between the redox potentials of the bridge and remote redox centers.

The standard heterogeneous electron-transfer rate constant, $k°$, depends on both a frequency factor and a Franck−Condon barrier[29−31]

$$k° = A_{et} \exp(-\Delta G^{‡}/RT) \quad (5)$$

where A_{et} is the preexponential factor and $\Delta G^{‡}$ is the electrochemical free energy of activation.[32]

It is important to decouple the free energy and preexponential terms since the effect of changing bridge states will be reflected in A_{et} rather than $\Delta G^{‡}$. One approach to decoupling these two contributions is to use classical temperature-resolved measurements of $k°$ to measure the free energy of activation, $\Delta G^{‡}$, allowing A_{et} to be determined. In this way, information about the strength of electronic coupling can be obtained. A second method involves measuring electron-transfer rate constants at a single temperature over a broad range of reaction driving forces. For example, Finklea,[33] Chidsey,[34] Creager,[35] and Murray,[36] have assembled nonadiabatic electron tunneling models that provide a good description of electron tunneling in monolayers of this kind.[37] In this model, the cathodic rate constant is given by the integral over energy (ϵ) of three functions: (a) the Fermi function for the metal $n(\epsilon)$, (b) a Gaussian distribution of energy levels for acceptor states in the monolayer $D_{ox}(\epsilon)$, and (c) a probability factor for electron tunneling, P

$$k_{ox}(\eta) = A \int_{-\infty}^{\infty} D_{ox}(\epsilon) n(\epsilon) P \, d\epsilon \quad (6)$$

The zero point of energy is defined as the Fermi level of the metal at the particular overpotential of interest. The Fermi function describes the distribution of occupied states within the metal and is defined by

$$n(\epsilon) = \left(\frac{1}{1 + \exp[(\epsilon - \epsilon_F)/k_B T]} \right) \quad (7)$$

where k_B is the Boltzmann constant. The density of acceptor states is derived from the Marcus theory[38] and is represented by eq 8

$$D_{ox}(\epsilon) = \exp\left[- \frac{(\epsilon + \eta - \lambda)^2}{4k\lambda T} \right] \quad (8)$$

where λ is the reorganization energy. The distance-dependent probability of electron tunneling is given by eq 9

$$P = \exp(-\beta d) \quad (9)$$

where d is the electron-transfer distance. The distance-dependent tunneling parameter, β, depends on the molecular structure of the bridging ligand,[39,40] but a value of 1.2 Å^{-1} is taken here as being representative of through-bond electron tunneling.[33]

The current for the reaction of an immobilized redox center following first-order kinetics is[36]

$$i_F = nFA(k_{ox}(\eta)\Gamma_{red,\eta} - k_{red}(\eta)\Gamma_{ox,\eta}) \quad (10)$$

where $\Gamma_{red,\eta}$ and $\Gamma_{ox,\eta}$ are the instantaneous surface coverages of the oxidized and reduced species and $k_{ox}(\eta)$ and $k_{red}(\eta)$ are the reaction rate constants given by eq 6 or its compliment in which $n(\epsilon)$ is replaced with $(1 - n(\epsilon))$ and $-\lambda$ is replaced by $+\lambda$ in eq 8. Energy-minimized molecular modeling indicates that the through-bond electron-transfer distance is approximately 7.6 Å. Therefore, when eq 10 is used to model the voltammetric response, there are only two freely adjustable parameters, $k°$ and $\Delta G^{‡}$ (λ/4). To model the experimental cyclic voltammograms, we have used the Nelder and Mead Simplex[41] algorithm to find the values of $k°$ and $\Delta G^{‡}$ that minimize the sum square

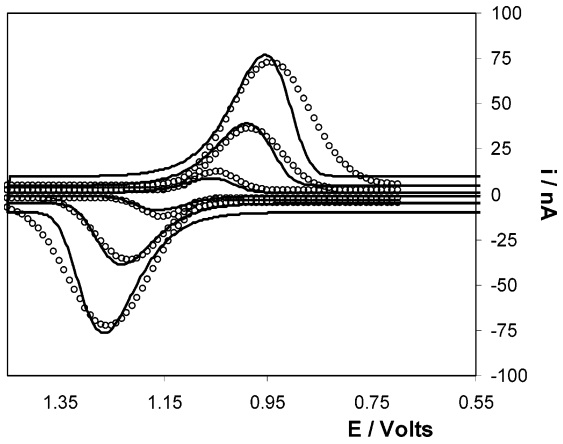

Figure 5. Cyclic voltammograms for a spontaneously adsorbed RuBpySH monolayer on a 2.5 μm radius platinum microdisk electrode where the scan rates from top to bottom are 10 000, 5000, and 1000 V s^{-1}. The open circles denote optimized theoretical fits to the data using a nonadiabatic electron tunneling model in which λ is 23.2 kJ mol^{-1} and k° is $0.9 \pm 0.1 \times 10^4$ s^{-1}.

residuals between the theoretical and the experimental currents observed in anodic branches of the linear sweep voltammograms.

Figure 5 shows that experimental and theoretical peak potentials and peak currents agree with one another to within experimental error for $\upsilon < 5000$ V s^{-1}. However, there are subtle differences in the experimental and theoretical peak shapes. For example, at a scan rate of 10 000 V s^{-1} the experimental response is noticeably sharper than is theoretically predicted. For $100 \leq \upsilon \leq 10\,000$ V s^{-1}, the optimum $\Delta G^\ddagger$ found is 5.8 ± 1.1 kJ mol^{-1}. For this system, the reorganization energy is likely to be dominated by outer sphere reorganization since bond lengths and angles are rather insensitive to the oxidation state of the metal center. Assuming that the optical and static dielectric constants of water are appropriate to describe the microenvironment within the monolayer and ignoring imaging effects, the Marcus theory[42,43] indicates that $\Delta G^\ddagger$ should be approximately 5.9 kJ mol^{-1}, which is indistinguishable from that found experimentally. However, the quality of the fit shown in Figure 5 is not particularly sensitive to $\Delta G^\ddagger$; e.g., increasing $\Delta G^\ddagger$ by 30% increases the residual sum of squares between the predicted and experimental peak currents by less than 10%. Therefore, while fitting of the cyclic voltammograms provides a convenient approach for determining k°, for this system it provides only an approximate value for $\Delta G^\ddagger$. In contrast, the quality of the fit is very sensitive to k°, which directly influences both the peak shape and the half-wave potential.

The best fits for voltammograms recorded at scan rates between 100 and 10 000 V s^{-1} is obtained with a k° value of $0.9 \pm 0.1 \times 10^4$ s^{-1}. The fact that voltammograms spanning 2 orders of magnitude in time scale can be fit by a single rate constant indicates that the monolayers are acceptably kinetically monodisperse. However, it is perhaps important to note that at higher scan rates, e.g., 10 000 V s^{-1}, the theoretical peak potential occurs at a more extreme value than that found experimentally. This observation suggests that there may be a small population of fast redox centers within the assembly.[33]

The magnitude of the rate constant is within an order of magnitude of that found for structurally related systems, e.g., where the bridging ligand is 4,4′-dipyridyl, 6-bis(4-pyridyl)-1,2,4,5-tetrazine, or 3,5-bis(pyridin-4-yl)-1,2,4-triazole.[44−46] However, it is more than 2 orders of magnitude slower that the electron-transfer rate constant found for ferrocene or $[Ru(NH_3)_5]^{2+}$ moieties linked through peptide coupling chemistry to an electrode surface under similar electron-transfer distances.[33,34,47] Weak electronic coupling between the ruthenium redox center and the electrode is a likely explanation of the observed behavior.

For an adiabatic reaction, the prefactor, A_{et}, is the product of κ_{el} the electronic transmission coefficient and υ_n a frequency factor dictated by either nuclear or solvent motion. In contrast, for a nonadiabatic reaction where the reactants are weakly coupled κ_{el} is significantly less than unity, and the prefactor is dictated by the electron hopping frequency in the activated complex, υ_{el}.[32] Electronic interaction of the redox orbitals and the metallic states causes splitting between the product and the reactant hypersurfaces that is quantified by H_{AB}, the matrix coupling element. The Landau−Zener treatment[48] of a nonadiabatic reaction yields eq 11

$$\upsilon_{el} = (2H_{AB}{}^2/h)(\pi^3/\lambda RT)^{1/2} \qquad (11)$$

where h is Planck's constant. The matrix coupling element obtained for the RuBpySH system is less than 1 kJ mol^{-1}, confirming that the system is always charge-localized and that there is very limited orbital mixing between the Ru^{2+} center and the platinum electrode.[48] While this very weak mixing is the most likely origin of the slow heterogeneous electron-transfer rate constants and near-surface emission observed, other factors, e.g., the short electron-transfer distance, mean that the electron-transfer event may take place within the electric field of the double layer.

Conclusions

Stable monolayers of $[Ru(bpy)_2(bpySH)](PF_6)_2$, RuBpySH, have been formed on micro and macro platinum electrodes by spontaneous adsorption from micromolar solutions of the complex in 50:50 v/v water/acetone. The adsorbed monolayers exhibit well-defined voltammetric responses for the $Ru^{2+/3+}$ switching process. The adsorption dynamics can be described using an irreversible adsorption model, and a single rate constant describes the behavior across a wide range of time scales and bulk concentrations. The monolayers emit light at 605 nm when the electrogenerated Ru^{3+} monolayer is exposed to tripropylamine. The ECL spectrum is similar in wavelength of maximum emission and peak shape to that found for photoluminescence, suggesting that the same orbitals are responsible whether the excited state is formed electrochemically or photochemically. The observation of emission, despite the luminophores sitting only 8 Å or so above a metal surface, is consistent with investigations of the heterogeneous electron-transfer process that indicate weak adsorbate−electrode interactions.

Acknowledgment. Funding from the European Union under the Marie Curie Research Training Network "UNI-NANO-CUPS" (MRTN-CT-2003-504233), COST D31, and the Science Foundation Ireland under the Biomedical Diagnostics Institute (Award No. 05/CE3/B754) is deeply appreciated. The generous loan of ruthenium trichloride and microwires by Johnson-Matthey is gratefully acknowledged.

References and Notes

(1) Whitesides, G. M.; Mathias, J. P.; Seto, C. T. *Science* **1991**, *254*, 1312.
(2) Ulman, A. *Chem. Rev.* **1996**, *96*, 1533.
(3) Cohen, M. L. *Mater. Sci. Eng., C* **2001**, *15*, 1.
(4) Karpovich, D. S.; Blanchard, G. J. *Langmuir* **1994**, *10*, 3315.
(5) Pan, W.; Durning, C. J.; Turro, N. J. *Langmuir* **1996**, *12*, 4469.

(6) Bain, C. D.; Troughton, E. B.; Tao, Y.-T.; Evall, J.; Whitesides, G. M.; Nuzzo, R. G. *J. Am. Chem. Soc.* **1989**, *111*, 321.
(7) Bensebaa, F.; Voicu, R.; Huron, L.; Ellis, T. H.; Kruus, E. *Langmuir* **1997**, *13*, 5335.
(8) Peterlinz, K. A.; Georgiadis, R. *Langmuir* **1996**, *12*, 4731.
(9) Dannenberger, O.; Buck, M.; Grunze, M. *J. Phys. Chem. B* **1999**, *103*, 2202.
(10) Hu, K.; Bard, A. J. *Langmuir* **1998**, *14*, 4790.
(11) Frubose, C.; Doblhofer, K. *J. Chem. Soc., Faraday Trans.* **1995**, *91*, 1949.
(12) Ron, H.; Rubinstein, I. *J. Am. Chem. Soc.* **1998**, *120*, 13444.
(13) Subramanian, R.; Lakshminarayanan, V. *Electrochim. Acta* **2000**, *45*, 4501.
(14) Dennany, L.; Forster, R. J.; Rusling, J. F. *J. Am. Chem. Soc.* **2003**, *125*, 5213.
(15) Dennany, L.; Forster, R. J.; White, B.; Smyth, M.; Rusling, J. F. *J. Am. Chem. Soc.* **2004**, *126*, 8835.
(16) Otsuki, J.; Kameda, H.; Tohimira, S.; Sakaguchi, H.; Takido, T. *Chem. Lett.* **2002**, 610.
(17) Obeng, Y. S.; Bard, A. J. *Langmuir* **1991**, *7*, 195.
(18) Kuwahara, Y.; Akiyama, T.; Yamada, S. *Thin Solid Films* **2001**, *393*, 273.
(19) Faulkner, L. R.; Walsh, M. R.; Xu, C. In *Contemporary Electroanalytical Chemistry*; Ivaska, A., Lewenstam, A., Rolf, S., Eds.; Plenum Press: New York, 1990; p 5.
(20) Magennis, S. W.; Parsons, S.; Pikramenou, Z. *Chem.—Eur. J.* **2002**, *8*, 5761.
(21) Alcock, N. W.; Barker, P. R.; Haider, J. M.; Hannon, M. J.; Painting, C. L.; Pikramenou, Z.; Plummer, E. A.; Rissanen, K.; Saarenketo, P. *J. Chem. Soc., Dalton Trans.* **2000**, 1447.
(22) Schubert, U. S.; Eschbaumer, C.; Hochwimmer, G. *Synthesis* **1999**, 779.
(23) Sullivan, B. P.; Salmon, D. J.; Meyer, T. J. *Inorg. Chem.* **1978**, *17*, 3334.
(24) Combellas, C.; Dellerue, S.; Mathey, G.; Thiébault, A. *Tetrahedron Lett.* **1997**, 539.
(25) Shimazu, K.; Yagi, I.; Sato, Y.; Uosaki, K. *Langmuir* **1992**, *8*, 1385.
(26) Juris, A.; Balzani, V.; Barigelletti, F.; Campagna, S.; Belser, P.; von Zelewsky, A. *Coord. Chem. Rev.* **1988**, *84*, 85.
(27) Caspar, J. V.; Meyer, T. J. *J. Am. Chem. Soc.* **1983**, *105*, 5583.
(28) Knight, A. W.; Greenway, G. M. *Analyst* 121, 101R.
(29) Bagchi, G. *Annu. Rev. Chem.* **1989**, *40*, 115.
(30) Sutin, N. *Acc. Chem. Res.* **1982**, *15*, 275.
(31) Barr, S. W.; Guyer, K. L.; Li, T. T.-T.; Liu, H. Y.; Weaver, M. J. *J. Electrochem. Soc.* **1984**, *131*, 1626.
(32) Sutin, N.; Brunschwig, B. S. *ACS Symp. Ser.* **1982**, *198*, 105.
(33) Finklea, H. O.; Hanshew, D. D. *J. Am. Chem. Soc.* **1992**, *114*, 3173.
(34) Chidsey, C. E. D. *Science* **1991**, *251*, 919.
(35) Weber, K.; Creager, S. E. *Anal. Chem.* **1994**, *66*, 3164.
(36) Tender, L.; Carter, M. T.; Murray, R. W. *Anal. Chem.* **1994**, *66*, 3173.
(37) Forster, R. J.; Loughman, P. J.; Figgemeier, E.; Lees, A. C.; Hjelm, J.; Vos, J. G. *Langmuir* **2000**, *16*, 7871.
(38) Marcus, R. A. *J. Phys. Chem.* **1963**, *67*, 853.
(39) Finklea, H. O.; Ravencroft, M. S.; Snider, D. A. *Langmuir* **1993**, *9*, 223.
(40) Beratan, D. N.; Hopfield, J. J. *J. Am. Chem. Soc.* **1984**, *106*, 1584.
(41) Ebert, K.; Ederer, H.; Isenhour, T. L *Computer Applications in Chemistry: An Introduction for PC Users*; VCH Publishers: New York, 1989.
(42) Marcus, R. A. *J. Chem. Phys.* **1956**, *24*, 966.
(43) Marcus, R. A. *J. Phys. Chem.* **1963**, *67*, 853.
(44) Forster, R. J.; Keyes, T. E. *J. Phys. Chem. B* **2001**, *105*, 8829.
(45) Walsh, D. A.; Keyes, T. E.; Hogan, C. F.; Forster, R. J. *J. Phys. Chem.* **2001**, *105*, 2792.
(46) Walsh, D. A.; Keyes, T. E.; Forster, R. J. *J. Phys. Chem. B* **2004**, *108*, 2631.
(47) Acevedo, D.; Abruna, H. D. *J. Phys. Chem.* **1991**, *95*, 9590.
(48) Brunschwig, B. S.; Sutin, N. *Coord. Chem. Rev.* **1999**, *187*, 233.